JFM RAPIDS
journals.cambridge.org/rapids

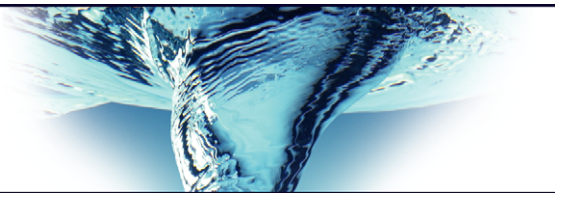

Lateral controls on grounding-line dynamics

Samuel S. Pegler†, Katarzyna N. Kowal, Leonard Q. Hasenclever and M. Grae Worster

Institute of Theoretical Geophysics, Department of Applied Mathematics and Theoretical Physics, Wilberforce Road, Cambridge CB3 0WA, UK

(Received 8 January 2013; revised 18 February 2013; accepted 3 March 2013; first published online 4 April 2013)

We present a theoretical and experimental study of viscous gravity currents introduced at the surface of a denser inviscid fluid layer of finite depth inside a vertical Hele-Shaw cell. Initially, the viscous fluid floats on the inviscid fluid, forming a self-similar, buoyancy-driven current resisted predominantly by the viscous stresses due to shear across the width of the cell. Once the viscous current contacts the base of the cell, the flow can be considered in two regions: a grounded region in which the current lies in full contact with the base; and a floating region. The subsequent advance of the grounding line separating these regions is shown to be controlled by the thickening of the current associated with balancing the local shear stresses. An understanding of the flow transitions is developed using asymptotic and numerical analysis of a model based on lubrication theory.

Key words: geophysical and geological flows, Hele-Shaw flows, ice sheets

1. Introduction

Ice sheets, such as those of Antarctica, flow viscously under their own weight at rates of several hundreds of metres per year, spreading gradually from the interior of the continent towards its periphery. Marine ice sheets are characterized by continuing to flow into the ocean and eventually detaching from the bedrock to form a floating *ice shelf*. Such configurations are common in West Antarctica, where the majority of the ice sheet lies on bedrock below sea level. Separating the grounded *ice sheet* and the ice shelf is the freely moving line of detachment called the *grounding line*, whose position corresponds approximately to where the thickness of the ice sheet has decreased to the depth of the ocean. Any thinning of the ice sheet at the grounding line, caused, for example, by the natural stretching of the flow towards the ocean due to buoyancy, leads to a retreat of the grounding line upstream. Such retreats have

† Email address for correspondence: ssp23@cam.ac.uk

doi:10.1017/jfm.2013.140

been observed in recent years (e.g. Wingham, Wallis & Shepherd 2009) and may be indications of a large-scale instability of the ice sheet, such as those which are known to have occurred in the geological past (Bamber *et al.* 2009).

Previous dynamical studies of marine ice sheets have focused predominantly on idealized two-dimensional cases in which the flow is assumed not to vary across its width (Weertman 1974; Wilchinsky & Chugunov 2000; Schoof 2007, 2011; Robison, Huppert & Worster 2010). In these studies, the sheet is modelled as a viscous gravity current whose flow is driven by gradients in hydrostatic pressure and resisted by friction at its base. In contrast, the absence of any significant friction at the base of the ice shelf implies that it instead forms an extensional viscous gravity current whose motion is resisted predominantly by the viscous stresses associated with its longitudinal extension (Weertman 1957; DiPietro & Cox 1979; Pegler & Worster 2012). Understanding the fluid mechanics associated with the transition between the sheet and shelf is challenging because the simplified thin-layer models that can be used to describe the leading-order flows of the sheet and shelf independently do not apply near the grounding line. In particular, if the friction at the base of the ice sheet is strong enough to induce significant vertical shear, then all the components of the stress tensor can be expected to become important near the grounding line (Nowicki & Wingham 2008; Schoof 2011). Attempts to model this system to date have mostly focused on cases where the sheet undergoes small vertical shear (Schoof 2007, 2011), on conducting a full-Stokes calculation of the steady flow (Nowicki & Wingham 2008), or on trying simplified descriptions of the dynamics in which certain leading-order stresses are neglected (Robison *et al.* 2010; Pegler & Worster 2013). In this paper, we demonstrate how additional viscous stresses that originate from the lateral confinement of marine ice sheets can lead to a new, simpler description of grounding-line migration.

When idealized to flow in two dimensions, an ice shelf simply transmits the hydrostatic pressure of the ocean through to the grounding line, so that the dynamics of the ice shelf itself have no influence on those of the sheet or grounding line (Weertman 1974; Schoof 2007; Robison *et al.* 2010). However, observations of the flow of ice following the collapse of an ice shelf have shown a subsequent acceleration of the grounded ice sheet that supplied it (e.g. Rignot *et al.* 2004), which suggests that ice shelves in fact play a role in buttressing the grounded ice sheet, resisting the flow of ice into the ocean and acting to stabilize the position of the grounding line. Such buttressing arises from the three-dimensional viscous stresses associated with deforming ice shelves through the embayments or channels in which they flow (Dupont & Alley 2005; Goldberg, Holland & Schoof 2009; Pegler & Worster 2012).

In this paper, our focus is to demonstrate how ice-shelf buttressing due to lateral stresses can lead to a different form of grounding-line migration in which the difficulties associated with the two-dimensional problem do not arise. To this end, we consider the idealized flow of a marine ice sheet between parallel sidewalls and develop a mathematical model for its evolution on the basis that the dominant resistance to flow arises from the viscous stresses associated with shearing across its width. Such flow regimes have been demonstrated to arise whenever an ice shelf becomes sufficiently longer than the width of the channel in which it flows (Pegler 2012). This configuration is typical of some ice shelves like the Amery Ice Shelf, which can be observed to undergo an approximately parabolic transverse velocity profile characteristic of Poiseuille flow (Budd 1966). Although most ice shelves do not flow in long channels, the fundamental controls identified in this paper relate to one end of a spectrum of ice-shelf geometries, with the strongly confined cases considered

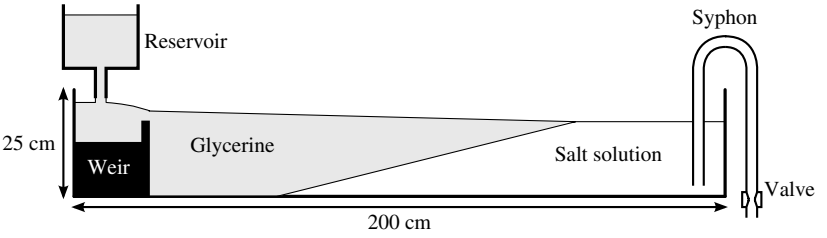

FIGURE 1. Schematic of our experimental system.

here at one end, and the very wide, essentially two-dimensional, cases (e.g. Schoof 2007) at the other. By comparing our results with those of two-dimensional studies, we elucidate the significant dynamical differences between these two extremes, with the expectation that either may play a partial or dominant role in any given geophysical setting.

We study the specific idealized system in which viscous fluid is supplied at a constant rate into a vertical Hele-Shaw cell filled to a constant depth by an inviscid fluid of greater density. The propagation of the viscous fluid through the cell is driven by gravity and resisted by transverse shearing across the width of the cell. Such flows have been studied previously in cases where the current remains in full contact with the base of the cell, primarily as an analogue for gravity-driven flows in porous media (Huppert 1986). Although this geometry leads to a flow that is much thicker than it is wide, this does not invalidate its applicability to ice shelves, as the regime of transverse-shear-dominated flow emerges for floating viscous layers of this kind irrespective of the ratio between the thickness and the width of the flow (Pegler 2012). While glacial ice is typically modelled as a shear-thinning, power-law fluid, the simpler Newtonian model we adopt describes the same fundamental fluid-mechanical forces, whilst being relatively easy to characterize in the laboratory using simple fluids.

We begin in § 2 by describing our experimental set-up and visual observations of a viscous fluid layer injected into a Hele-Shaw cell filled with denser inviscid fluid. In § 3, we develop a theoretical model of the flow and explore the model equations using both numerical and asymptotic approaches. In § 4, we compare the data with our theoretical predictions. Finally, in § 5 we discuss the implications of our results for grounding-line dynamics in the geophysical setting.

2. Experimental observations

We developed an experimental analogue of a confined marine ice sheet using a vertical Hele-Shaw cell formed of two Perspex sheets of length 200 cm and height 25 cm (see figure 1). The mean spacing $w \approx 1.35$ cm of the cells was determined by filling the cell with a known volume of water and dividing this by the length of the cell and the depth of the water body. By also measuring the spacing directly at various locations using a pair of callipers, we estimated that the spacing deviated slightly from the mean value by a maximum of about 0.05 cm. We used glycerine of density $\rho \approx 1.26$ g cm^{-3}, dyed with blue food colouring, to form the viscous current, and solutions of potassium carbonate with larger densities of up to $\rho_w \approx 1.56$ g cm^{-3} to form the inviscid fluid layer. The viscosity of the glycerine was measured before each experiment using a glass U-tube viscometer, and varied slightly between experiments

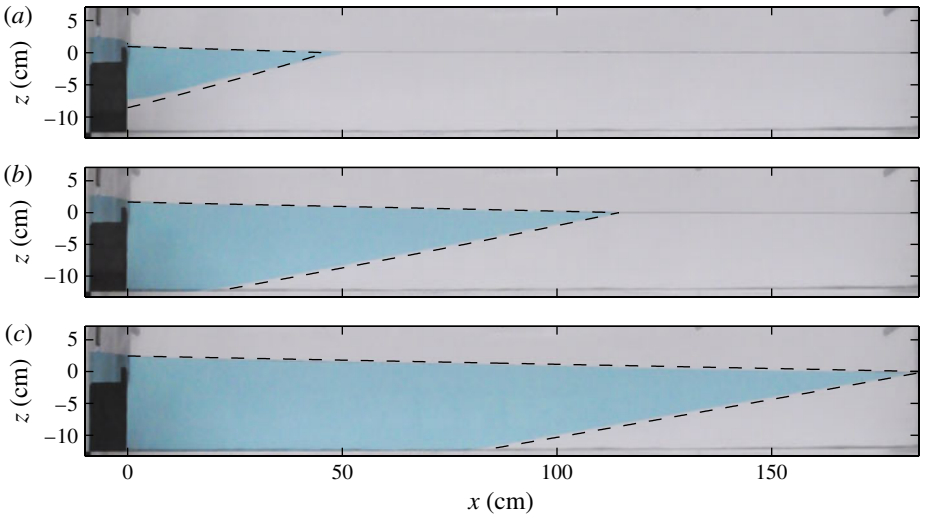

FIGURE 2. Sequence of photographs showing the experimental evolution of the viscous current of glycerine (dyed blue) above a denser solution of potassium carbonate at times $t = 60,\ 240$ and 480 s after the initiation of the injection. The theoretically predicted positions of the surfaces of the current are shown as dashed curves in each panel. The experiment is also shown in supplementary movie 1.

owing to differences in water content. The injection of glycerine into the cell was achieved through a vertical steel tube connected to a suspended reservoir. The tube was directed to supply glycerine above a weir secured inside the cell, with the constancy of the injection rate maintained during each experiment by keeping the head in the reservoir at a constant level.

To set up the experiment, the cell was initially filled with potassium carbonate solution to a depth b, such that the top surface of the solution lay approximately 1 cm below the top of the weir. The injection of glycerine was then initiated, causing it to fill the space behind the weir and then spill over it – see figure 2 and supplementary movie 1 (available at http://dx.doi.org/10.1017/jfm.2013.140) To counteract the rise in the depth of the solution caused by its displacement by the glycerine, we extracted solution manually through a syphon located at the opposite end of the cell to the injection. The extraction was performed whenever the level could be determined by eye to have exceeded its initial height, giving an accuracy of depth b to within 0.5 cm. The experiment was recorded using a camera directed towards the front of the cell. Note that any effects due to surface tension, which are most significant near the front of the current, can be expected to be negligible once the current is much thicker than the capillary length scale (Pegler, Lister & Worster 2012), which we estimate to be of the order of millimetres for currents produced by our experimental system.

The evolution of one of our experiments is shown as a time-lapse sequence in figure 2 and supplementary movie 1. The glycerine is first seen to float entirely over the inviscid fluid, producing a dynamical analogue of a confined *shelf*. At a certain time, the floating current makes contact with the base of the cell to form the grounded *sheet*, which lies in full contact with the base. The contact line separating the sheet and shelf, or *grounding line*, subsequently propagates along the base of the cell over the course of the experiment.

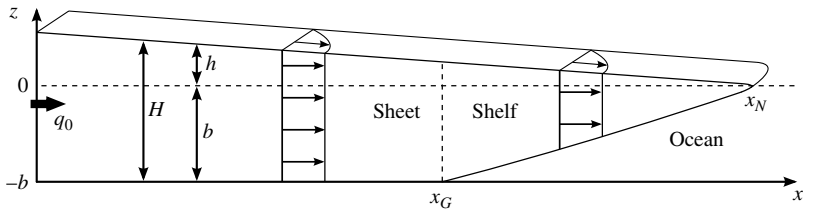

FIGURE 3. Schematic cross-section of a viscous fluid layer confined between vertical sidewalls and above a lower boundary at $z = -b$.

3. Theoretical model

Consider a layer of viscous Newtonian fluid of density ρ and kinematic viscosity ν flowing in a vertical Hele-Shaw cell of width w filled to a constant depth b by an inviscid fluid of higher density ρ_w (see figure 3). Our experimental observations in § 2 indicated that the layer forms two regions: the floating shelf in $x_G < x < x_N$, and the grounded sheet in $0 < x < x_G$, where $x_N(t)$ and $x_G(t)$ represent the frontal position of the shelf and the grounding line, respectively. Let $h(x, t)$ denote the height of the upper surface of the current above the surface of the inviscid fluid $z = 0$, and let $H(x, t)$ denote the thickness of the current. These are related by

$$h = H - b \qquad (0 < x < x_G), \tag{3.1a}$$

$$h = (\Delta\rho/\rho_w)H \quad (x_G < x < x_N), \tag{3.1b}$$

where $\Delta\rho \equiv \rho_w - \rho$. Equation (3.1*a*) follows from the fact that the vertical position of the base of the sheet is set simply by the geometry of the underlying surface. Equation (3.1*b*) follows from the assumption that the vertical position of the shelf is set by Archimedes principle (cf. Robison *et al.* 2010; Pegler & Worster 2013).

We develop a model of the flow under the assumption that the leading-order resistance to flow originates from the viscous stresses associated with shearing across the width of the cell. In such cases (cf. Huppert 1986), the horizontal and vertical components of the Stokes equations with dynamic viscosity $\mu \equiv \rho\nu$ can be simplified to

$$\mu u_{yy} = p_x, \quad p_z = -\rho g, \tag{3.2a,b}$$

respectively, where we have used subscripts to denote partial differentiation, a notation which we also extend to derivatives of time t below. To this end, we assume that the width of the cell is much less than both the thickness and extent of the current, so

$$w \ll H, \quad w \ll x_N. \tag{3.3a,b}$$

Assumption (3.3*a*) has been applied previously to model the transverse-shear-dominated flow of a fully grounded current (Huppert 1986), where it implies that the vertical shear stresses that would dominate the dynamics in the case of a wide channel are confined to a small boundary layer at the base of the cell (Happel & Brenner 1991). By contrast, this assumption is not needed to ensure the dominance of transverse shear stresses in the shelf, as the absence of any traction along its lower surface implies that vertical shear stresses are automatically negligible. Instead, transverse-shear-dominated flow in the shelf depends only on the assumption (3.3*b*) that it is much longer than it is wide (Pegler 2012). This ensures that the viscous extensional stresses that would dominate the dynamics of a wide shelf

(cf. Robison *et al.* 2010) remain negligible compared with transverse shear stresses ($u_{xx} \ll u_{yy}$). In particular, the shear-dominated regime of the shelf would then apply even if its thickness were much less than its width ($H \ll w$), as is relevant to the geophysical setting.

With the possible exception of narrow ice streams, stresses due to transverse shear, assumed to be dominant in our model, are unlikely to provide the dominant resistance to the flow of the grounded component of the ice sheet in the geophysical setting, where stresses due to vertical shear are more likely to dominate (e.g. Robison *et al.* 2010). However, the dynamics of transverse- and vertical-shear-dominated viscous gravity currents are physically similar, with only minor differences between the nonlinear diffusion equations that govern them. Therefore, we do not expect this distinction to affect the essential dynamics explored in this paper, which are more closely tied to the ice shelf.

By integrating (3.2*a*) subject to no-slip conditions at the cell walls, and using the integrated form of (3.2*b*) to substitute for the leading-order hydrostatic pressure, we determine the volumetric flux per unit width of the cell as

$$q = -\frac{gw^2}{12\nu} H h_x = -\frac{\tilde{g} w^2}{12\nu} H H_x, \tag{3.4a,b}$$

where

$$\tilde{g} \equiv g \quad (0 < x < x_G), \tag{3.5a}$$

$$\tilde{g} \equiv g' \quad (x_G < x < x_N), \tag{3.5b}$$

and $g' \equiv (\Delta\rho/\rho_w)g$ is the reduced gravity. Equation (3.4*a*) has been developed previously by Huppert (1986), while (3.4*b*) follows on using (3.1) to substitute for h in (3.4*a*). Using (3.4*b*) to evaluate q in the depth-integrated form of the continuity equation, we obtain the governing nonlinear diffusion equation

$$H_t = \frac{w^2}{12\nu} (\tilde{g} H H_x)_x, \tag{3.6}$$

where $\tilde{g}$ acts as a piecewise-constant coefficient of diffusion.

At the source, we impose a condition of constant volumetric flux, namely,

$$q = q_0 \quad (x = 0), \tag{3.7}$$

where q_0 is a constant. At the grounding line, we impose conditions of continuity on the thickness and the flux

$$H^+ = H^- = d, \quad q^+ = q^- \quad (x = x_G), \tag{3.8a,b}$$

respectively, where $d \equiv \rho_w b/\rho$ is the *flotation thickness*. Condition (3.8*a*) is a dynamic condition, which describes a balance between the depth-integrated longitudinal stresses across the grounding line, which are hydrostatic to leading order. This dynamic condition is considerably simpler than those that have been developed previously in two-dimensional models (e.g. Schoof 2007; Robison *et al.* 2010), where the transition towards an extensional flow at the grounding line implies that the leading-order longitudinal stress is not hydrostatic. Note that a condition of identical form to (3.8*a*) is also applied in those models, but there it acts instead as an initial condition on solutions to the higher-order hyperbolic equation that governs the evolution of the shelf.

Finally, we assume that the frontal thickness of the current vanishes and that its position evolves kinematically according to

$$H = 0, \quad \dot{x}_N = -\frac{g' w^2}{12\nu} H_x \quad (x = x_N), \tag{3.9a,b}$$

where we use a dot to denote $\mathrm{d}/\mathrm{d}t$.

We make the system (3.6)–(3.9) dimensionless by defining

$$x \equiv \mathscr{L}\hat{x} \equiv \left(\frac{g d^2 w^2}{12\nu q_0}\right)\hat{x}, \quad t \equiv \mathscr{T}\hat{t} \equiv \left(\frac{g d^3 w^2}{12\nu q_0^2}\right)\hat{t}, \quad H \equiv d\,\hat{H}. \tag{3.10a,b,c}$$

The time scale $\mathscr{T}$ in (3.10*b*) characterizes the time on which the sheet thickens by d, and the length scale $\mathscr{L}$ in (3.10*a*) characterizes the distance propagated by the sheet in that time. In terms of (3.10*a*,*b*,*c*) and with hats dropped, (3.6) becomes

$$H_t = (HH_x)_x \qquad (0 < x < x_G), \tag{3.11}$$

$$H_t = \epsilon\,(HH_x)_x \quad (x_G < x < x_N), \tag{3.12}$$

and conditions (3.7)–(3.9) become

$$q = 1 \qquad (x = 0), \tag{3.13}$$

$$H^+ = H^- = 1, \quad H_x^+ = \epsilon H_x^- \qquad (x = x_G), \tag{3.14a,b}$$

$$H = 0, \quad \dot{x}_N = -\epsilon H_x \quad (x = x_N), \tag{3.15a,b}$$

respectively. The system above depends on the single dimensionless parameter

$$\epsilon \equiv \frac{g'}{g} \equiv \frac{\Delta\rho}{\rho_w}, \tag{3.16}$$

which is a dimensionless density difference. For ice floating on water, $\epsilon \approx 0.1$.

An illustrative solution to the system (3.11)–(3.15) in the case $\epsilon = 0.1$ is shown at a progression of times as dashed curves in figure 2, and the corresponding evolutions of the grounding line $x_G(t)$ and frontal position $x_N(t)$ are shown as solid curves in figure 4 and compared with experimental data in figure 5. Once the injection is initiated, the entire current initially floats over the inviscid fluid, as illustrated in figure 2(*a*). During this initial phase, the flow is described entirely by the shelf equations (3.12), (3.13) and (3.15). By suitably scaling t by ϵ, these equations reduce to those developed previously to describe a fully grounded current (Huppert 1986), for which they are found to support a similarity solution of the form

$$H = (t/\epsilon)^{1/3} f(x/x_N), \quad x_N = a\,(t/\epsilon)^{2/3} \quad (t < T), \tag{3.17a,b}$$

where $a \approx 1.48$ and $f(x/x_N)$ is a nearly linear function, as indicated in figure 2(*a*).

The prediction of self-similar flow (3.17*a*,*b*) breaks down once the lower surface of the current makes contact with the base of the cell or, equivalently, once $H = 1$. On setting $x = 0$ and $H = 1$ in (3.17*a*), we determine the *time of grounding* as

$$T \equiv f\,(0)^{-3}\,\epsilon \approx 0.46\epsilon. \tag{3.18}$$

Once $t \geqslant T$, a sheet forms in the region $0 < x < x_G$, with the grounding line x_G advancing from $x = 0$, as illustrated in figure 2(*b*). The flow then conforms to the intrinsic scales in (3.10*a*,*b*,*c*), precluding any subsequent self-similarity. To determine the evolution for $t > T$, we solve (3.11)–(3.15) numerically using a second-order, partially implicit finite-difference scheme in which the domains of the sheet and shelf

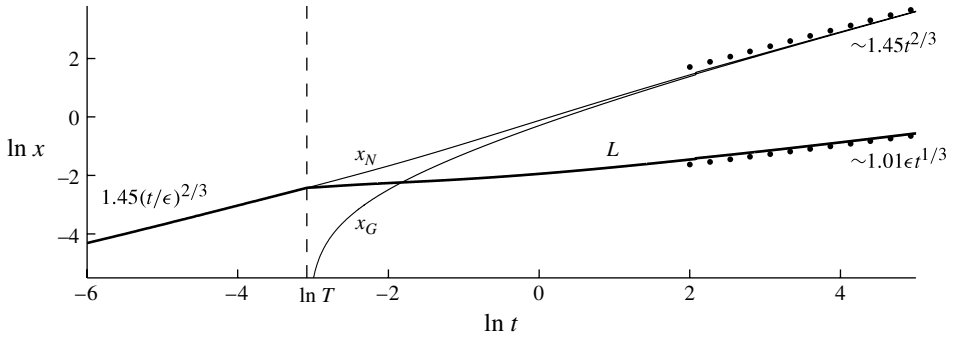

FIGURE 4. Evolution of the grounding line $x_G(t)$, frontal position $x_N(t)$ (both thin curves) and shelf length $L(t) \equiv x_N - x_G$ (thick curve) for $\epsilon = 0.1$, with the asymptotes (3.20*b*) and (3.21) shown as dotted lines.

are each mapped onto fixed grids. To avoid numerical instabilities associated with the changing of the domain, we employed a two-step method in which the first step is used to predict the rates of change of the boundaries, $\dot{x}_G$ and $\dot{x}_N$.

As shown by figures 4 and 5, the grounding line x_G advances abruptly from $x = 0$ with a finite velocity, and the rate at which the length of the shelf $L(t) \equiv x_N - x_G$ increases is suddenly reduced. Beyond a time of order ϵ, the sheet occupies a significantly larger proportion of the current than the shelf ($L \ll x_G$) and the grounding line becomes controlled kinematically by the rate at which fluid is supplied towards it, so $\dot{x}_G \sim -H_x^-(x_G, t)$. With $\epsilon \ll 1$, this regime of kinematic control is established rapidly on times of order unity ($t \gtrsim 1 \gg \epsilon$). The shelf is then effectively pushed forwards by the sheet, transitioning towards a state of uniform velocity $U(t) = -\epsilon H_x$, independent of x. Integrating this expression subject to (3.13), (3.14*a*) and (3.15*a*), we determine the asymptotic relationships

$$H \sim \frac{x_N - x}{L}, \quad L \sim \frac{\epsilon}{q(x_G, t)} \quad (t \gg \epsilon), \tag{3.19a,b}$$

which show that the thickness (3.19*a*) becomes linearly distributed and the length (3.19*b*) becomes inversely proportional to the flux $q(x_G, t)$ delivered to the grounding line.

At later times ($t \gg 1$), the interior thickness of the sheet becomes much greater than the flotation thickness ($H \gg 1$), so the sheet can be expected to approach the asymptotic similarity solution of a fully grounded current (Huppert 1986), namely,

$$H \sim t^{1/3} f(x/x_G), \quad x_G \sim at^{2/3} \quad (t \gg 1), \tag{3.20a,b}$$

which is the same as (3.17), but with $\epsilon = 1$. Using (3.14) and (3.20) to evaluate the leading-order flux delivered to the grounding line as $q(x_G, t) = -HH_x^- \sim [-f'(1)/a]t^{-1/3}$, and then substituting this expression into (3.19*b*), we determine the late-time shelf length as

$$L \sim 1.01\epsilon t^{1/3} \quad (t \gg 1). \tag{3.21}$$

This confirms that the shelf grows with time, but at a slower rate than the sheet (3.20*b*), as illustrated by the dotted lines in figure 4.

If the shelf were removed at any stage, then the forces exerted at the grounding line would change dramatically. Specifically, with the sudden removal of the *buttressing*

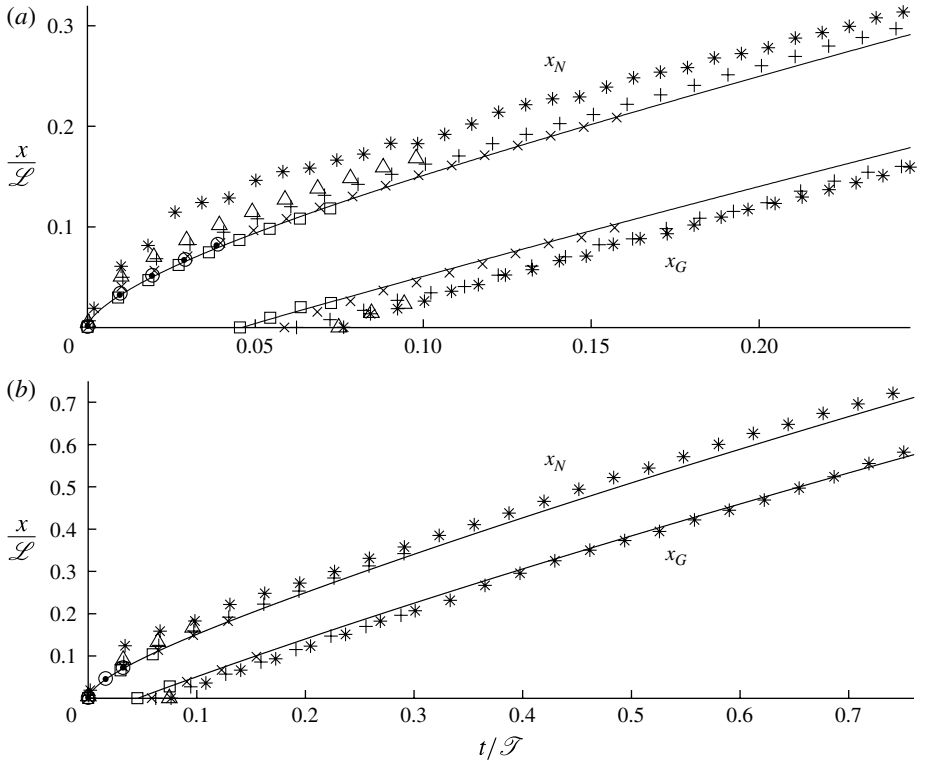

FIGURE 5. (*a*) Scaled experimental data for the frontal position $x_N(t)$ and grounding-line position $x_G(t)$ for the experiments having dimensionless density difference $\epsilon \approx 0.1$, as listed in table 1. (*b*) The same data as in panel (*a*) to larger times. The theoretical predictions are shown as solid curves.

force associated with pushing the ice shelf forwards at the grounding line, there would be an abrupt increase in the divergence of flux across it, causing the grounding line to retreat temporarily while the shelf is re-formed. Indeed, while our results predict that the grounding line advances indefinitely, models that involve no buttressing from the shelf (e.g. Weertman 1974) predict that the grounding line can retreat indefinitely upstream over horizontal bedrock, implying an instability of the ice sheet. Ice-shelf buttressing can therefore dictate the stability of a marine ice sheet.

4. Experimental comparison

Our experimental parameters spanned viscosities of $\nu \approx 4.8$ to $9.0\ \mathrm{cm^2\ s^{-1}}$, reduced gravities of $g' \approx 13$ to $190\ \mathrm{cm\ s^{-2}}$, input fluxes per unit width of $q_0 \approx 1.0$ to $14.8\ \mathrm{cm^2\ s^{-1}}$ and depths of the inviscid fluid of $b \approx 3.0$ to 17.5 cm (see table 1). The evolutions of the grounding line $x_G(t)$ and frontal position $x_N(t)$, determined by digitally detecting the outline of the glycerine in our recorded images, are plotted in terms of our dimensionless variables (3.10) in figure 5. We find good agreement with the theoretical prediction (solid curves).

The strength of agreement is seen to vary between our experiments. We expect that the discrepancy is due to a slight difference between the source flow produced by our experimental system and that which is imposed in our idealized theoretical model.

Symbol	ν (cm^2 s^{-1})	g' (cm s^{-2})	q_0 (cm^2 s^{-1})	b (cm)	ϵ	S
	5.4	13	1.1	12.0	0.013	0.17
	6.2	13	5.0	17.5	0.013	0.62
	5.5	13	6.3	17.5	0.013	0.69
	6.5	13	5.6	12.0	0.013	1.05
	6.6	13	5.3	7.0	0.013	1.74
	5.7	30	1.2	7.0	0.03	0.15
	7.4	30	6.2	17.5	0.03	0.40
	8.2	30	3.9	7.0	0.03	0.69
	6.4	50	1.0	7.0	0.05	0.08
	6.6	50	5.4	12.0	0.05	0.27
	6.8	50	4.9	7.0	0.05	0.43
	7.1	50	14.8	12.0	0.05	0.79
□	5.8	100	1.2	7.5	0.10	0.04
•	8.0	100	3.0	17.5	0.10	0.06
○	8.4	100	3.0	17.5	0.10	0.07
×	7.3	100	3.8	12.0	0.10	0.10
△	8.3	100	5.8	17.5	0.10	0.12
+	9.0	100	3.4	10.0	0.10	0.14
*	8.5	100	3.9	7.0	0.10	0.21
	4.8	190	2.5	7.0	0.19	0.04
	6.5	190	5.3	7.0	0.19	0.12
	6.3	190	7.1	7.0	0.19	0.15

TABLE 1. Parameter values used in our experiments.

Specifically, while our model presupposes that the flow is everywhere horizontal and that the source flow is distributed uniformly over the full depth of the current, the experimental source differed by distributing the injection through a small gap of the order of 1 cm at the top of the weir (see figure 2). In effect, this imposed a point source at the top of the weir, leading to an approximately radial velocity $u_r \sim 4(q_0/2\pi r)$, where r is the distance from the top of the weir. The flow therefore underwent a transition from a radial flow driven by a pressure gradient $\partial p/\partial r = -(12\mu/w^2)u_r$, towards a buoyancy-driven regime of predominantly horizontal flow. By forming a scaling between $\partial p/\partial r$ and the hydrostatic pressure gradient of the buoyancy-induced flow, $\partial p/\partial z \sim \rho g'$, we determine the characteristic extent of this transition region as $r \sim \mathscr{R} \equiv (24/\pi)(\nu q_0/g'w^2)$, beyond which the influence of the radial pressure gradient at the source can be expected to be unimportant. To measure the significance of $\mathscr{R}$ across our experiments, we consider its ratio with b, namely,

$$S \equiv \frac{\mathscr{R}}{b} \equiv \frac{24}{\pi}\frac{\nu q_0}{g'w^2 b}, \tag{4.1}$$

which is listed for each of our experiments in table 1. To examine the relationship between the discrepancy and S, we have plotted as circles the time of grounding T as a function of ϵ across all our experiments in figure 6, where the area of each circle is proportional to S, and we have plotted the theoretical prediction (3.18) as a solid line. We observe a general trend of smaller S leading to smaller discrepancy, providing confirmation that the source flow is indeed the likely cause of the discrepancy. Moreover, the experimental values of T generally overshoot the predictions, reflecting the fact that the isolation of the source at the top of the weir naturally leads to less of the fluid plunging below the weir, as illustrated in figure 2(*a*). The progression of errors in the times to grounding illustrated by figure 6 can also be seen between the

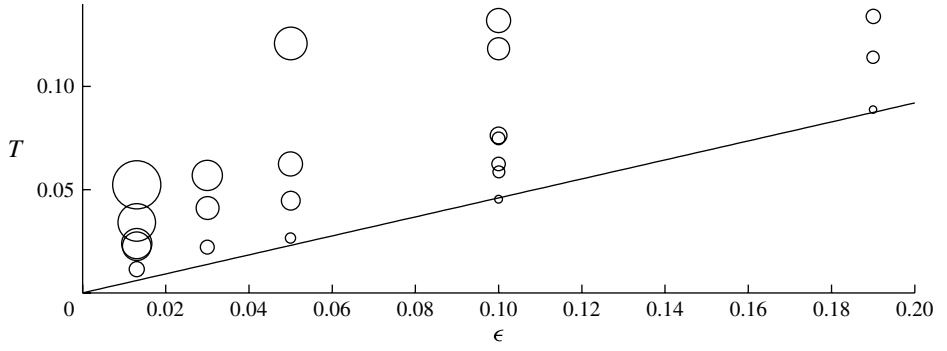

FIGURE 6. Dimensionless time T for the current to make contact with the base plotted as a function of the dimensionless density difference ϵ for each of our experiments (circles). The area of each circle is proportional to the dimensionless source strength S defined by (4.1), as given in table 1. The theoretical prediction (3.18) is shown as a solid line.

sets of data in figure 5. Here, the absolute error between the predicted and observed positions of the grounding line are seen to remain approximately constant at larger times, eventually becoming small relative to the position of the grounding line.

5. Conclusions

We have explored the dynamics of confined marine ice sheets by developing a model in which the dominant resistance to flow originates from the stresses associated with driving the flow through the geometry. In the specific case of a uniform ocean depth, we showed that, after a preliminary self-similar regime in which the current floats entirely over the inviscid fluid, a grounding line forms and proceeds to advance indefinitely. Data from a series of laboratory experiments showed good agreement with our theoretical predictions.

Our results suggest a new mechanism for how the position of the grounding line can be established in situations where a marine ice sheet is confined laterally. Specifically, given the volumetric flux entering the ice shelf at the grounding line, we found that the position of the grounding line is determined simply by the point at which the shear-dominated regime of the ice shelf, as modelled by the theory we have developed, predicts that the ice shelf intersects the bedrock. Remarkably, and in strong contrast to two-dimensional marine ice sheets (cf. Weertman 1974; Schoof 2007), the position of the grounding line is determined independently of the dynamics of the sheet upstream of the grounding line, and depends only on geometry and the flux delivered into the ice shelf.

Acknowledgements

We are grateful to Mark Hallworth, Colin Hitch and David Page-Croft for assistance in setting up our experiments. K.N.K. is grateful for a summer studentship provided by James Bridgewater. L.Q.H. is grateful for support provided by an EPSRC summer studentship and Jesus College, Cambridge.

Supplementary movie

Supplementary movie is available at http://dx.doi.org/10.1017/jfm.2013.140

References

BAMBER, J. L., RIVA, R. E. M., VERMEERSEN, B. L. A. & LEBROQ, A. M. 2009 Reassessment of the potential sea-level rise from a collapse of the West Antarctic Ice Sheet. *Science* **324** (5929), 901–903.

BUDD, W. F. 1966 The dynamics of the Amery Ice Shelf. *J. Glaciol.* **5**, 335–358.

DIPIETRO, N. D. & COX, R. G. 1979 The spreading of a very viscous liquid on a quiescent water surface. *Q. J. Mech. Appl. Maths* **32**, 355–381.

DUPONT, T. K. & ALLEY, R. B. 2005 Assessment of the importance of ice-shelf buttressing to ice-sheet flow. *Geophys. Res. Lett.* **32**, F03009.

GOLDBERG, D., HOLLAND, D. M. & SCHOOF, C. 2009 Grounding line movement and ice shelf buttressing in marine ice sheets. *J. Geophys. Res.* **114**, F0402.

HAPPEL, J. & BRENNER, H. 1991 *Low Reynolds Number Hydrodynamics: with Special Applications to Particulate Media*, 2nd edn. Kluwer Academic.

HUPPERT, H. E. 1986 The intrusion of fluid mechanics into geology. *J. Fluid Mech.* **173**, 557–594.

NOWICKI, S. M. J. & WINGHAM, D. J. 2008 Conditions for a steady ice sheet–ice shelf junction. *Earth Planet. Sci. Lett.* **265**, 246–255.

PEGLER, S. S. 2012 The fluid mechanics of ice-shelf buttressing. PhD thesis, University of Cambridge.

PEGLER, S. S., LISTER, J. R. & WORSTER, M. G. 2012 Release of a viscous power-law fluid over a denser inviscid ocean. *J. Fluid Mech.* **700**, 261–281.

PEGLER, S. S. & WORSTER, M. G. 2012 Dynamics of a viscous layer flowing radially over an inviscid ocean. *J. Fluid Mech.* **696**, 152–174.

PEGLER, S. S. & WORSTER, M. G. 2013 An experimental and theoretical study of the dynamics of grounding lines. *J. Fluid Mech.* (submitted).

RIGNOT, E., CASASSA, G., GOGINENI, P., KRABILL, W., RIVERA, A. & THOMAS, R. 2004 Accelerated ice discharge from the Antarctic Peninsula following the collapse of Larsen B ice shelf. *Geophys. Res. Lett.* **31**, L18401.

ROBISON, R. A. V., HUPPERT, H. E. & WORSTER, M. G. 2010 Dynamics of viscous grounding lines. *J. Fluid Mech.* **648**, 363–380.

SCHOOF, C. 2007 Marine ice-sheet dynamics. Part 1. The case of rapid sliding. *J. Fluid Mech.* **573**, 27–55.

SCHOOF, C. 2011 Marine ice-sheet dynamics. Part 2. A Stokes flow contact line problem. *J. Fluid Mech.* **679**, 122–255.

WEERTMAN, J. 1957 Deformation of floating ice shelves. *J. Glaciol.* **3**, 38–42.

WEERTMAN, J. 1974 Stability of the junction of an ice sheet and an ice shelf. *J. Glaciol.* **31**, 3–11.

WILCHINSKY, A. V. & CHUGUNOV, V. A. 2000 Ice stream–ice shelf transition: theoretical analysis of two-dimensional flow. *Ann. Glaciol.* **30**, 153–162.

WINGHAM, D., WALLIS, D. & SHEPHERD, A. 2009 Spatial and temporal evolution of Pine Island Glacier thinning. *Geophys. Res. Lett.* **36**, L17–501.